Jagannath University Journal of Science
Volume 08, Number II, June 2022, pp. 15–26
https://jnu.ac.bd/journal/portal/archives/science.jsp
ISSN 2224-1698

JnUJSci

Heat and Mass Transfer Simulation of MHD Radiative Flow of Casson Fluid Through an Inclined Stretching Surface

Research Article

Sarder Firoz Ahmmed[*1], Kausari Sultana[2] and Md. Mehedi Hasan Rasel[1]

[1]*Mathematics Discipline, Khulna University, Khulna-9208, Bangladesh.*

[2]*Department of Mathematics, Shahjalal University of Science and Technology, Sylhet-3114, Bangladesh*

Received: 22 March 2022
Accepted: 10 May 2022

Abstract: The heat and mass transfer nature of Magneto hydrodynamics (MHD) radiative flow of Casson fluid through an inclined stretching surface is investigated in the presence of magnetic field, chemical reaction, thermal radiation. The governing nonlinear system of partial differential equations are transformed into system of couple ordinary differential equations. This transformation is done by using similarity transformation and suitable physical non-dimensional parameters. This is solved numerically by using Runge-Kutta sixth order with Nachtsheim-Swigert iteration technique and displayed graphically by using Tecplot 9.0. The effects of velocity, temperature and concentration for various parameters are discussed. The friction factor, rate of heat transfer and rate of mass transfer are also explained graphically. Fluid's flow, heat exchange, mass transfer and skin friction drops while Nusselt number and rate of mass exchange are rises as Casson fluid parameter grows. On the other hand, temperature increases for chemical reaction parameter, mass Grashof number, magnetic parameter, exponential parameter, Prandtl number while falls for radiation parameter and Schmidt number.

Keywords: *Casson fluid • Magnetohydrodynamics • Non- Newtonian fluid • Runge-Kutta method*

1. Introduction

Non-Newtonian fluids become a great attention to researchers. There is a great importance in industries such as chemicals, cosmetics, food, oil, gas, pharmaceuticals, wire and fiber coating, design of heat exchangers and several branches of engineering applications especially in paper production, hot rolling, metal spinning, plastic polymer, photodynamic therapy, bio-medicine and in several situations such as prediction of space weather, damping of turbulent fluctuations etc. So, the importance is enormous in different area of science and technology. Casson fluid is a liquid of shear thinning. Casson fluid is accurately applicable to silicon suspensions, bentonite suspensions and lithographic varnishes. Casson fluid model is a simple differential type model. In 1959, Casson gave this model for the flow of viscoelastic fluids. In both very high and very low shear rates, the Casson model is more accurate.

Heat and mass transfer phenomena in the flow of Casson fluid over an infinite oscillating plate in the presence of first-order chemical reaction and slip effect by Saqib *et al.* (2016). In their paper, the model was modeled in terms of partial differential equations. Coupled ordinary differential equations were then solved by Laplace transform method. They studied the velocity profile for different parameters through numerical computation and are displayed by graph. They analyzed the analytic and exact solution. Sulochana *et al.* (2021) made an effort to

* Corresponding Author: Sarder Firoz Ahmmed
Email: sfahmmed@yahoo.com

figure out the heat and mass transfer of MHD Casson fluid flow over a wedge with thermal radiation and chemical reaction. The flow governing equations were transformed into ordinary differential equations. They analyzed the couple equations by using Runge-Kutta numerical approach with a shooting technique. Various physical parameters were graphically outlined and computed by MATLAB software. They studied the comparative study between Casson fluid and Newtonian fluid and they found that Casson fluid displays superior heat transfer than the Newtonian fluid.

Reddy (2015) presented the unsteady radiative convective boundary layer flow of a Casson fluid with variable thermal conductivity. They transformed the time-dependent governing partial differential equations into coupled nonlinear ordinary differential equations. Then the transformed equations were solved numerically by using shooting method. They analyzed the effects of thermal radiation and thermal conductivity on the unsteady Casson fluid flow. The effects were examined on some polymer solutions. Hydromagnetic flow past a continuously moving semi-infinite plate for large suction by Singh and Dikshit (1988). The perturbation method was used for the similarity equations and the equations were solved analytically. They found that skin friction increases with the increase of magnetic parameter. Alam *et al.* (2006) presented the numerical study of the combined free-forced convection and mass transfer flow past a vertical porous plate in a porous medium with heat generation and thermal diffusion. They solved the nondimensional governing equation numerically by applying Nachtsheim-Swigert shooting iteration technique together with Runge-Kutta sixth order integration scheme. They studied the effects of suction parameter, heat generation parameter and Soret number on the flow field.

Asogwa and Ibe (2020) made an effort to figure out the study of MHD Casson fluid flow over a permeable stretching sheet with heat and mass transfer. The system of PDE was transformed into system of ODE by suitable similarity transformation and solved numerically by MATLAB bvp4c solver. They analyzed the influence of various physical parameters on the flow of fluid, temperature, concentration. They found that flow, heat and mass transfer have significant effect. MHD Casson fluid flow through a vertical plate was investigated by Parandhama *et al.* (2019). They solved the non-dimensional multivariable governing equations by using Runge-Kutta scheme along with shooting technique. They studied the impacts of different pertinent parameters on velocity and temperature. Bali and Awasthi (2012) developed the Casson fluid model for multiple stenosed artery in the presence of magnetic field.

The exact solutions for unsteady free convective flow of Casson fluid over an oscillating vertical plate with constant wall temperature was computed by Khalid *et al.* (2015). Laplace transform method was used for numerical analysis. They obtained the impacts of different embedded parameters on velocity, temperature, concentration. They provided the numerical analysis and analytical analysis for skin friction and Nusselt number. Pramanik (2013) described the Casson fluid flow and heat transfer past an exponentially porous stretching surface in presence of thermal radiation. Runge-Kutta fourth order method was used for the numerical analysis. He investigated the combined effects of suction and thermal radiation. He found that velocity and heat transfer were influenced by pertinent parameters in the presence suction/blowing at the wall. He also discussed the skin friction for different parameters.

Haq *et al.* (2014) investigated the convective heat transfer and MHD effects on Casson nanofluid flow over a shrinking sheet. Along with boundary conditions the system of non-linear PDE were transformed into system of multivariable ODE by applying suitable similarity transformations. They solved the transformed equations numerically by Runge-Kutta method. Effects of different parameters are examined for velocity, heat transfer and were displayed through graphs and tables. They provided the fluid flow behavior through stream lines. Unsteady boundary layer flow and heat transfer of a Casson fluid past an oscillating vertical plate with Newtonian heating was studied by Hussanan *et al.* (2014). The governing system of equations were transformed to a systems of linear partial differential equations by using suitable non-dimensional variables. The resulting equations were solved analytically by Laplace transform technique. They found that with the increase Casson parameters velocity decreases and thermal boundary layer thickness increases with the increase of Newtonian heating parameter.

Obeide and Hammodat (2020) discussed the new study of the stability of fluid flow in a porous channel under effects of magnetic field and radiation. They investigated the stability analysis in the case of the variable amplitude. They found that the physical parameters had significant effect on the stability of the system. Nadeem *et al.* (2013) studied the MHD three-dimensional Casson fluid flow past a porous linearly stretching sheet. They found that the dimensionless velocities and shear stresses in both directions. Pertinent results were provided graphically and quantitatively with respect to the variation in Casson flow parameter.

The boundary layer flow of Casson nanofluid over a vertical exponentially stretching cylinder was investigated by Malik *et al.* (2014). Using suitable similarity

transformations the governing multivariable system of partial differential equations were transformed into system of nonlinear ordinary differential equations. Runge-Kutta Fehlberg method was used to solve the resulting system numerically. They examined the natural convection parameter and other physical parameter through graphs. Nadeem *et al.* (2012) made an effort to figure out the MHD flow of a Casson fluid over an exponentially shrinking sheet. The analytical solution was carried out by adomain decomposition method. They used the diagonal approximant for the validity of the convergent. Effects of pertinent physical parameters on velocity profiles are described.

Khalid *et al.* (2015) obtained unsteady MHD free convection flow of Casson fluid past over an oscillating vertical plate embedded in a porous medium. The non-dimensional equations are solved using Laplace transform technique. There is a sine and cosine oscillations were expressed in terms of exponential and complementary error functions for exact solutions. They evaluated the skin friction and Nusselt number and results for different parameters. The optimized analytical solution for oblique flow of a Casson nanofluid with convective boundary conditions was investigated by Nadeem *et al.* (2014). The transformed system of ODE from system of PDE were solved analytically using Optimal Homotopy analysis method via BVPh2.0. The profiles of velocity, temperature and concentration were expressed through graph. They provided the physical behaviors of pertinent parameters.

Sarojamma *et al.* (2014) studied the MHD Casson fluid flow, heat and mass transfer in a vertical channel with stretching walls. They used the Runge-Kutta fourth order shooting method for numerical solution. They showed that with the increase magnetic field strength, the velocity of the decreases. They also provided the investigation in the study of blood flow in the cardiovascular system. An analysis on the dual solutions of Casson fluid flow over a stretching or shrinking sheet was conducted by Kameswaran *et al.* (2014). They also investigated the effects of Soret and Dufour parameters. They used the MATLAB bvp4c package for the numerical solutions and for negative stretching parameter, dual solutions for velocity, temperature, concentration were obtained. They also provided the nature of skin friction, heat and mass transfer rate for Casson parameter.

Vijaya *et al.* (2016) surveyed the electromagnetic field's impact on the energy transmission flow in a Casson narrow film on an unstable expanding plane. They investigated the influences of Lorentz force, dissipation of viscosity and heating internally. For various pertinent parameters, the distributions of velocity and temperature were obtained in thin film. Unsteady flow of a hydromagnetic Casson fluid enclosed alongside with two collateral non conducting permeable plates was investigated by Wahiduzzaman *et al.* (2014). Reduced non-dimensional system of PDE were figured out numerically by Crank-Nicolson method. They discussed the flow for various parameters.

Magnetohydrodynamics radiation flux flow of Casson and Williamson nanofluids over an inclined columnar surface with synthetic reaction influence was explored by Sarkar *et al.* (2019). They used the algorithm of compact visual FORTRAN and explicit finite difference method was applied for the analysis. Convergence criterion was also provided in this paper. Impact of Casson and Williamson parameters were also depicted via isotherms and streamlines. They found that nature of velocity profile and heat transfer profile of Williamson fluid was relatively lower than that of Casson fluid. Computational modelling of multiphase behavior over a stretching sheet in the presence of nanoparticles was inquired by Reza-E-Rabbi *et al*. (2019). Raju *et al.* (2016) explored the mass transport and heat transmit in Magnetohydrodynamics Casson fluid on top of an exponentially absorbent stretching plane. They solved the transformed PDE by MATLAB bvp4c package. Fluid flow, temperature, mass along with friction factor, rates of mass transfer and heat transfer were discussed for different parameters.

Motivated by the above investigations, the present analysis is focused on the study of mass and heat transmit simulation of magnetohydrodynamics energy flux flow of Casson fluid via leaned stretching plane. Numerical solutions are obtained by sixth order Runge-Kutta method in company with Nachtsheim-Swigert shooting reiteration approach. Graphical results are presented and described for different relevant parameters. Graphical results are given for field of velocity, field of temperature and field of mass together with skin friction factor, rate of mass transfer and Nusselt number. Under few special circumstances the present work have a magnificent accord with the different investigations regarding Casson fluid.

2. Mathematical analysis

Consider a time invariant, incompressible, pressure-invariant hydromagnetic Casson fluid flow through an inclined and past a nonlinear exponentially stretching sheet which is initially at rest is considered. A non-uniform field of magnet with strength B_0 is applied. The flow of the fluid is confined to $y > 0$.The current investigation has a low magnetic Reynolds number. There is no electric field in this study. Chemical reaction is also assumed with above consideration. The *x*- axis is subjected to two opposing and equal forces.

Aforementioned forces keep the origin fixed in addition to the wall remains stretched. The viscoelastic equation for an incompressible Casson fluid is correspond as,

$$\tau_{ij} = \begin{cases} 2\left(\mu_B + \dfrac{p_y}{\sqrt{2\pi}}\right)e^{ij}, & \pi > \pi_c \\ 2\left(\mu_B + \dfrac{p_y}{\sqrt{2\pi}}\right)e^{ij}, & \pi < \pi_c \end{cases}$$

where μ be the dynamic viscosity, σ be the shear rate, $\pi = e_{ij}e_{ij}$ and e_{ij} expresses (i, j) part of distorsion rate, μ_B designates the plastic dynamic viscosity, p_y be the yielding stress, π be the multiplication of the element of rate of distorsion and the critical value of the aforementioned product is π_c.

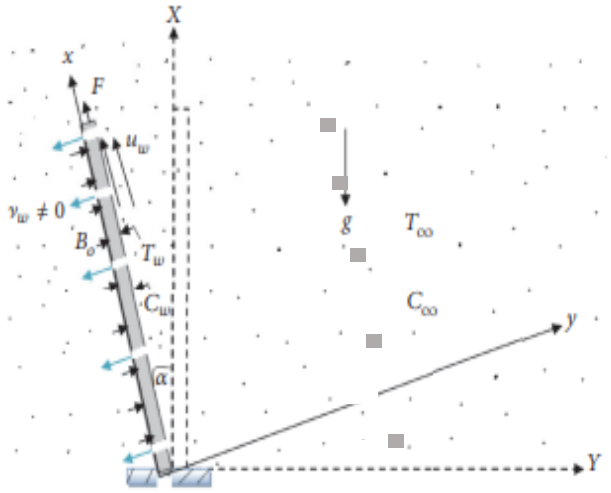

Figure 1. Flow near the inclined stretching sheet.

Under the above suppositions along with the Boussineq's boundary layer estimations, the model governs the continuity equation, momentum equation, energy and concentration equations are given by (1) to (4) as

$$\frac{\partial u}{\partial x} + \frac{\partial v}{\partial y} = 0 \tag{1}$$

$$u\frac{\partial u}{\partial x} + v\frac{\partial u}{\partial y} = \nu\left(1 + \frac{1}{\beta}\right)\frac{\partial^2 u}{\partial y^2} + g\beta_T(T - T_\infty)\cos + g\beta_c(C - C_\infty)\cos\alpha - \frac{\sigma B^2 u}{\rho} \tag{2}$$

$$u\frac{\partial T}{\partial x} + v\frac{\partial T}{\partial y} = \frac{k}{\rho c_P}\frac{\partial^2 T}{\partial y^2} - \frac{1}{\rho c_P}\frac{\partial q_r}{\partial y} + \frac{\mu}{\rho c_P}\left(1 + \frac{1}{\beta}\right)\left(\frac{\partial u}{\partial y}\right)^2 \tag{3}$$

$$u\frac{\partial C}{\partial x} + v\frac{\partial C}{\partial y} = D_B\frac{\partial^2 C}{\partial y^2} - k_e(C - C_\infty) + \frac{D_m K_T}{T_m}\frac{\partial^2 T}{\partial y^2} \tag{4}$$

the boundary conditions are given in equation (5),

$$u = U,\ v = -V(x),\ T = T_w,\ C = C_w \text{ at } y = 0$$
$$u \to 0,\ T \to T_\infty,\ C \to C_\infty \text{ as } y \to \infty \tag{5}$$

where u and v are the components of velocity in the directions of x and y respectively, the Casson fluid parameter is β, heat transfer is for T, the mass transfer of the fluid be C, ρ be the fluid density, ν be the viscosity of kinematics, g be the gravitational acceleration, β_T be the thermal expansion coefficient, β_c be the concentration expansion coefficient, σ be the conductivity of heat, T_∞ be the free flowing stream temperature, C_∞ be the free flowing stream concentration, Variable field of magnet be B, k be the conductivity of heat, the specific heat of the fluid at invariable pressure be c_P, ρc_P be the fluid's heat reactance, q_r be the thermal radiation flux, μ be the dynamic viscosity, D_m be the coefficient of mass diffusivity, k_e be the parameter of chemical reaction, and $V(x)$ be the suction or injection parameter.

q_r, the radiation heat flux is put together with the Rosseland's estimation is given in equation (6),

$$q_r = -\left(\frac{4\sigma^*}{3k_1}\right)\frac{\partial T^4}{\partial y} \tag{6}$$

where, σ^* be the Stefan- Boltzmann constant, k_1 be the coefficient of absorption. Extending T^4 about T_∞ and then ignoring the higher sequence terms apart from first degree of T. Therefore, the rate of heat flux exchange with regard to y is given in equation (7),

$$\frac{\partial q_r}{\partial y} = -\left(\frac{16T_\infty^3\sigma^*}{3k_1}\right)\frac{\partial^2 T}{\partial y^2} \tag{7}$$

Substitution of equation (7) into the second term which changes equation (3) into the equation (8),

$$u\frac{\partial T}{\partial x}+v\frac{\partial T}{\partial y}=\frac{k}{\rho c_P}\frac{\partial^2 T}{\partial y^2}+\frac{1}{\rho c_P}\frac{16\sigma T_\infty^3}{3k^*}\frac{\partial^2 T}{\partial y^2}$$

$$+\frac{\mu}{\rho c_P}\left(1+\frac{1}{\beta}\right)\left(\frac{\partial u}{\partial y}\right)^2 \quad (8)$$

Now employing the similarity transformation to the PDEs (2), (8) and (4) transfigured into a simultaneous ordinary differential equation is given in equation (9),

$$\eta=\sqrt{U_0/2\nu L}\,e^{Nx/2L}y,\ v=-\sqrt{\nu U_0/2L}\,e^{Nx/2L}Nf(\eta),\ u=U_0e^{Nx/L}f'(\eta),$$

$$T=T_\infty+T_0e^{2Nx/L}\theta,\ C=C_\infty+C_0e^{2Nx/L}\phi \quad (9)$$

where, T_∞ be the free stream temperature, C_∞ be the surrounding concentration, L be the characterized length, U_0 be the flow of the fluid, N be the exponential parameter.

The dimensionless equations are given in equations (10), (11) and (12) as,

$$\left(1+\frac{1}{\beta}\right)f'''+N\left(ff''-2f'^2\right)+2Gr\theta\cos\alpha$$

$$+2Gc\phi\cos\alpha-Mf'=0 \quad (10)$$

$$\frac{1}{\Pr}(R+1)\theta''+N\left(-4f'\theta+f\theta'\right)+\left(1+\frac{1}{\beta}\right)Ecf''^2=0 \quad (11)$$

$$\phi''+NSc\left(f\phi'-4\phi f'\right)$$

$$-Sc\,kr\,\phi+ScSr\theta''=0 \quad (12)$$

The transformed/deduced boundary conditions are given by equation (13),

$$f(\eta)=f_w,\ f'(\eta)=1,\ \theta(\eta)=1,\ \phi(\eta)=1 \text{ at } y=0$$

$$f'(\eta)\to 0,\ \theta\to 0,\ \phi\to 0 \text{ as } y\to\infty \quad (13)$$

where the parameters are given as,

Casson fluid parameter, $\beta=\mu_B\sqrt{2\pi_c}/p_y$, magnetic field parameter, $M=\sigma B_0^2/\rho u_0$, thermal Grashof number, $Gr=g\beta LT_0/U_0^2$, exponential parameter, N, mass/ solutal Grashof number, $Gc=g\beta LC_0/U_0^2$, Prandtl number, $\Pr=\nu/k=c_P\mu/k$, radiation parameter, $R=16\sigma^*T_\infty^3/3k^*k$, Eckert number, $Ec=U_0^2/T_0c_P$, Schmidt number, $Sc=\nu/D_B$, chemical reaction parameter, $kr=k_eL/C_0U_0$.

The expressions for coefficient of skin friction, local Nusselt number and local Sherwood number are,

$$Cf_x=\left(1+\frac{1}{\beta}\right)\frac{\tau_w}{\rho U_0^2},\qquad Nu_x=\frac{xq_w}{k(T_w-T_\infty)},$$

$$Sh_x=\frac{xq_m}{D_B(C_w-C_\infty)}$$

where τ_w is the wall shear stresses along x- direction and q_w and q_m are the flux of heat and flux of mass respectively are given by $q_w=-k\left(\frac{\partial T}{\partial y}\right)_{y=0}$,

$$q_m=-D_B\left(\frac{\partial C}{\partial y}\right)_{y=0}$$

The physical expressions with ample applications in the engineering field which are termed as local skin friction factor (Cf_x), coefficient of heat transfer (Nu_x) and Sherwood number (Sh_x) are taking the dimensionless form in the equation (14) as,

$$Cf_x\,\mathrm{Re}_x^{1/2}=\left(1+1/\beta\right)f''(0),\ Nu_x\,\mathrm{Re}_x^{-1/2}=-\theta'(0),$$

$$Sh_x\,\mathrm{Re}_x^{-1/2}=-\phi'(0) \quad (14)$$

where $\mathrm{Re}_x=(xU_0e^{Nx/L})/\nu$ is the local Reynolds number.

3. Numerical Analysis

To solve the governing coupled non-dimensional partial differential equations with the associated initial and boundary conditions. The method of Runge-kutta sixth order with Nachtsheim-Swigert shooting iteration technique has been used to solve equations (10–12) subject to the initial and boundary conditions. In this there are three asymptotic boundary condition and hence three unknown surface conditions are $f''(0)$, $\theta'(0)$ and $\phi'(0)$ .The outer boundary conditions are given by the equation (15),

Now choose,

$$f'(\eta_{\max}) = f'(f''(0), \theta'(0), \phi'(0)) = \delta_1, \quad \theta(\eta_{\max}) = \theta(f''(0), \theta'(0), \phi'(0)) = \delta_2$$
$$\phi(\eta_{\max}) = \phi(f''(0), \theta'(0), \phi'(0)) = \delta_3, \quad f''(\eta_{\max}) = f''(f''(0), \theta'(0), \phi'(0)) = \delta_4$$
$$\theta'(\eta_{\max}) = \theta'(f''(0), \theta'(0), \phi'(0)) = \delta_5, \quad \phi'(\eta_{\max}) = \phi'(f''(0), \theta'(0), \phi'(0)) = \delta_6 \tag{15}$$

Considering, $f''(0) = g_1, \theta'(0) = g_2, \phi'(0) = g_3$ and the minimum value of the error is calculated by,

$$E = \delta_1^2 + \delta_2^2 + \delta_3^2 + \delta_4^2 + \delta_5^2 + \delta_6^2 \tag{16}$$

In order to get the solutions as an initial value problem, we need the values of $f''(0), \theta'(0)$ and $\phi'(0)$, but there is no such values in the boundary. The most important factor of shooting method is to find the appropriate finite values for η_∞. In order to determine that values for η_∞, starting with some initial guess value for some particular set of physical parameters to obtain $f''(0)$ and $\theta'(0)$ and $\phi'(0)$. The technique is repeated with a larger value of η_∞ until the difference between successive values of $f''(0), \theta'(0)$ and $\phi'(0)$ is only significant digit satisfying the boundary conditions. The choosen last value of η_∞ is the most appropriate value for η_∞ for particular set of parameters. This may change for another set of pertinent parameters. The process is completed once the finite value of η_∞ has been determined. After each iteration, it is required to satisfy the boundary conditions and in order to get a better approximation for the solution, adjust the approximated values.

The numerical value of the independent variable is used to approach infinity in the trial integration. There is no single best strategy for estimating these values. Large values cause the trial integration to diverge or the surface boundary conditions to slowly converge. In terms of computer time, selecting too large values is costly. Nachtsheim-Swigert devised an iteration method for dealing with dealing with these problems. In order to get the solution Runge-kutta sixth order method with Nachtsheim-Swigert shooting iteration technique has been used with step size h = 0.01. The process repeated until the desired accuracy of degree 10^{-4} is obtained. Using these data, graphical representation is obtained for different parameters by Tecplot 9.0.

4. Results and discussion

The simultaneous nonlinear ordinary differential equations (10), (11) and (12) are resolved numerically with the assistance of Runge-Kutta sixth order method with Nachtsheim-Swigert iteration approach by Microsoft Visual Studio 2010 with FORTRAN scheme. The acquired results described the impacts of various dimensionless parameters, specifically magnetic field parameter (*M*), Eckert Number (*Ec*), Casson fluid parameter (β), exponential parameter (*N*), thermal Grashof number (*Gr*), mass Grashof number (*Gc*), Soret number (*Sr*), Prandtl number (*Pr*), Schmidt number (*Sc*), radiation parameter (*R*), angle of inclination (α) and chemical reaction parameter (*kr*) on the fluid flow, temperature and mass transfer. The skin friction, rate of heat transfer and Sherwood number are also described graphically. For numerical outcomes, the value of the main parameters are considered as β = 0.1, N = 0.05, Gr =1.0, Gc = 0.5, M =1.0, Ec = 0.1, Pr = 0.7, Sc =0.6, Sr = 0.1, kr = 0.5, R = 0.5 and α = 10. For illustrations of the results of the solution, the numerical data are depicted in Figs. 2-17. The validation of the results is presented in Table 1.

Figures 2 and 3 depict the effects of Casson fluid parameter on the field of temperature and mass exchange respectively. It is understandable that with the rise of Casson fluid parameter there is a fall of temperature. As a result of the fact that there is a drop in the thermal boundary layer when there is a rise of Casson fluid parameter. For η = 0.4, the temperatures are 0.8872, 0.8859 and 0.8844 for β = 0.1, β = 2.1 and β = 4.1 respectively. For β = 0.1 to β = 2.1 the rate of decrease is 0.065% and for β = 0.1 to β= 4.1 is 0.075%. As the Casson fluid parameter is increased, the fluid concentration drops. For β = 0.1, β=2.1 and β = 4.1 the concentrations are 0.8532, 0.8509 and 0.8487 respectively. The rate of decrement for β = 0.1 to β = 2.1 is 0.115% and the rate of decrement for β = 0.1 to β = 4.1 is 0.11%.

The impacts of Casson fluid parameter on heat transfer rate and mass exchange rate are demonstrated in Fig. 4 and Fig. 5 respectively. Nusselt number and mass transfer rate increases because of the rise of Casson fluid parameter. Nusselt numbers or rate of heat transfer are 0.3054, 0.3064 and 0.30738 for β = 0.1, β = 2.1 and β = 4.1 at η = 0.4. The rate of increment for β = 0.1 to β = 2.1 is 0.05% and rate of increment for β = 0.1 to β = 4.1 is 0.49%. Sherwood numbers or rate of mass transfer are 0.2915, 0.2933 and 0.2951 for β = 0.1, β = 2.1 and β = 4.1 at η = 0.4. For η = 0.4, the rate of increment for β = 0.1 to β = 2.1 is 0.09% and rate of increment for β = 0.1 to β = 4.1 is 0.09%.

The effects of exponential parameter on concentration

profiles are revealed in Fig. 6 There is a significant effect for exponential parameter and it is evident that concentration decreases with the rise of exponential parameter. This occurs due to the decline nature of thickness of concentration boundary layer and rise of thickness of thermal and momentum boundary layer. The concentration of the fluid falls when the exponential parameter is increased. For *N=1.0, N=2.0* and *N=3.0* the concentrations are 0.8532, 0.8048 and 0.7548. The rate of decrement for *N=1.0* to *N=2.0* is 10.76% and 10% is the decreasing rate for *N=1.0* to *N=3.0.*

Figure 7 displays the impacts of exponential parameter on mass exchange rate respectively. Sherwood numbers or rate of mass transfer are 0.2915, 0.2344 and 0.1778 for *N=1.0, N=2.0* and *N=3.0* respectively. For η = 0.6, the rate of decrement for *N=1.0* to *N=2.0* is 0.09% and rate of decrement for *N=1.0* to *N=3.0* is 0.09%. The impacts of *Gr* on the field of velocity is manifested in Fig. 8 It is obvious that fluid flow decreases as increase of *Gr*. This occurs due to the decline nature of the thickness of concentration boundary layer. The ratio of thermal buoyant force to hydrodynamic force is known as the thermal Grashof number. If thermal buoyancy force increases then it results in the increase of thermal Grashof number. When the hydrodynamic force increases, the thermal Grashof number decreases. For η=0.4, for thermal Grashof number *Gr = 1.0, Gr = 2.0* and *Gr = 3.0* the velocities are 0.8619, 0.8540 and 0.8462 respectively. For *Gr =1.0* to *Gr = 2.0* the rate of decrement is 0.79%. For *Gr =1.0* to *Gr = 3.0* the decreasing rate is 0.78%. The validation of the result is given in Table 1.

Table 1. Comparison of the values of $f''(0)$, $-\theta'(0)$ and $-\phi'(0)$ for various values of Pr.

	Raju et al. (2016)	**Nadeem et al. (2014)**	**Present study**
$f''(0)$	*D*	*D*	*D*
$-\theta'(0)$	*I*	*I*	*I*
$-\phi'(0)$	*D*	*D*	*D*

where *D* represents the decreasing rate and *I* represents the increasing rate.

Figures 9 and 10 display the outcome of mass Grashof number on velocity profiles and temperature respectively. It is apparent that velocity decreases and temperature increases with the increase of concentration Grashof number. For η = 0.6, for concentration Grashof number *Gc = 0.5, Gc = 1.5* and *Gc = 2.5* the velocities are 0.7338, 0.72003 and 0.7062. For *Gc = 0.5* to *Gc = 1.5* the rate of diminution is 1.377%. For *Gc = 0.5* to *Gc=2.5* the decreasing rate is 1.383%. For η = 0.6, the temperatures are 0.7872, 0.7874 and 0.7877 for *Gc = 0.5, Gc = 1.5* and *Gc = 2.5* respectively. For *Gc=0.5* to *Gc = 1.5* the rate of increment is 0.02% and for *Gc = 0.5* to *Gc = 2.5* is 0.03%.

The influences of Prandtl number on the field of velocity and field of temperature are revealed in Fig. 11 and Fig. 12 respectively. It is clear that velocity and temperature increases with the increase of Prandtl number. Prandtl number is the ratio of momentum diffusivity to thermal diffusivity. As a result of increase in momentum diffusivity, the velocity increases. The velocities for Prandtl number *Pr = 0.72, Pr = 2.36* and *Pr = 2.72* are 0.5038, 0.5534 and 0.559 for η = 1.0. The rate of increment for *Pr = 0.72* to *Pr = 2.36* is 3.02%. For *Pr = 0.72* to *Pr = 2.72* the increasing rate is 2.76%. For η = 1.0, the temperatures are 0.606, 0.766 and 0.792 for *Pr = 0.72, Pr = 2.36* and *Pr = 2.72* respectively. For *Pr = 0.72* to *Pr = 2.36* the rate of gain is 9.76% and for *Pr = 0.72* to *Pr = 2.72* is 9.3%. The effects of number of Soret on the field of velocity, temperature and mass disposed by Fig. 13, Fig. 14 and Fig. 15 respectively. With an increase in the number of Soret, fluid flow, heat and concentration all drops. For η = 0.6, for soret number *Sr = 0.1, Sr =1.1* and *Sr = 2.1* the velocities are 0.7338, 0.7243 and 0.7144. The rate of decrement for *Sr = 0.1* to *Sr =1.1* is 0.95%. For *Sr = 0.1* to *Sr = 2.1* the decreasing rate is 0.99%. For η = 0.6, the temperatures are 0.7872, 0.7752 and 0.7639 for *Sr = 0.1, Sr =1.1* and *Sr = 2.1* respectively. For *Sr = 0.1* to *Sr =1.1* the rate of decrement is 1.2% and for *Sr=0.1* to *Sr =2.1* is 1.13%. Concentration of the fluid decreases with the increase of soret number. For *Sr = 0.1, Sr = 1.1* and *Sr=2.1* the concentrations are 0.71304, 0.7025 and 0.6911. The rate of decrement for *Sr = 0.1* to *Sr = 1.1* is 1.054% and 1.14% is the decreasing rate for *Sr=0.1* to *Sr = 2.1.*

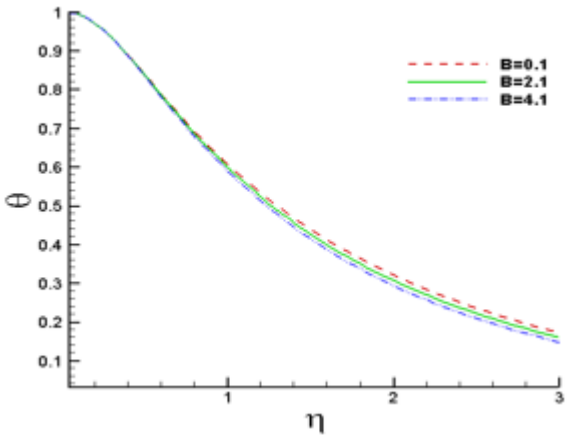

Figure 2. Impacts of various Casson fluid parameter on the field of temperature.

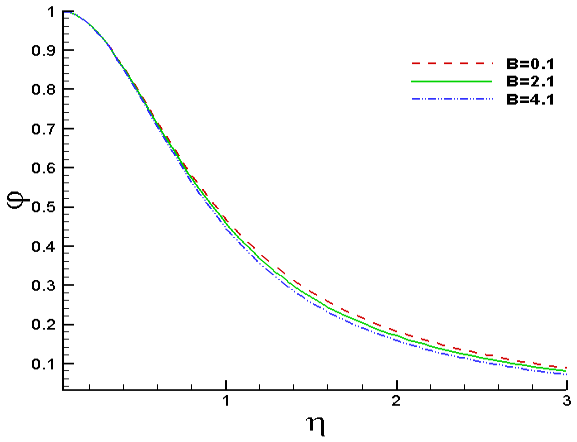

Figure 3. Impacts of various Casson fluid parameter on the field of concentration.

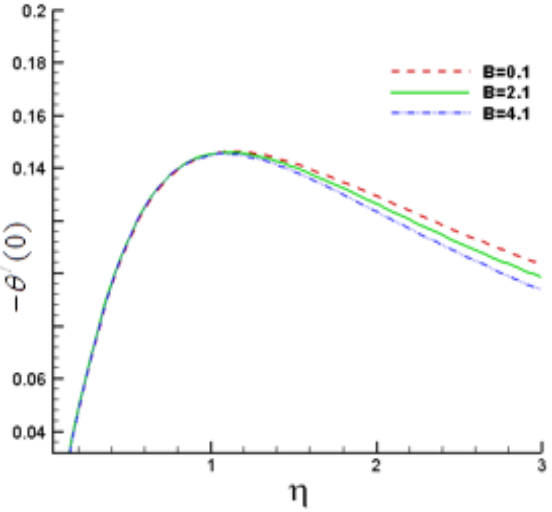

Figure 4. Impacts of various Casson fluid parameter on the rate of heat exchange.

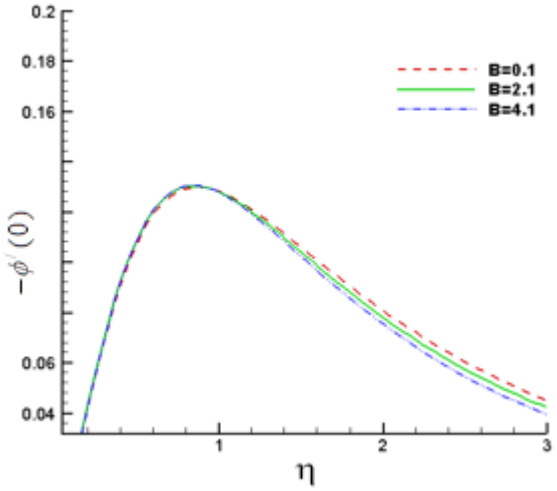

Figure 5. Impacts of various Casson fluid parameter on the rate of mass exchange.

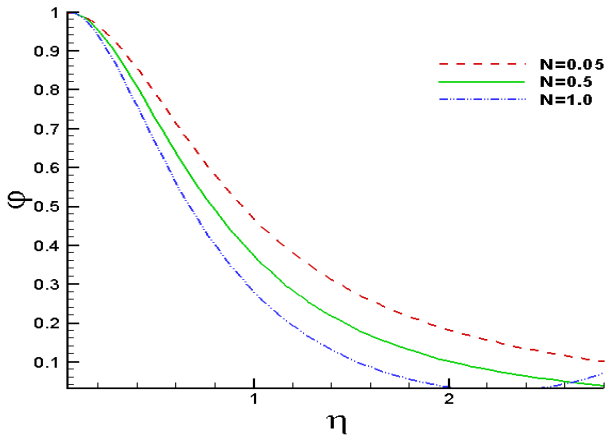

Figure 6. Impacts of various *N* on the field of concentration.

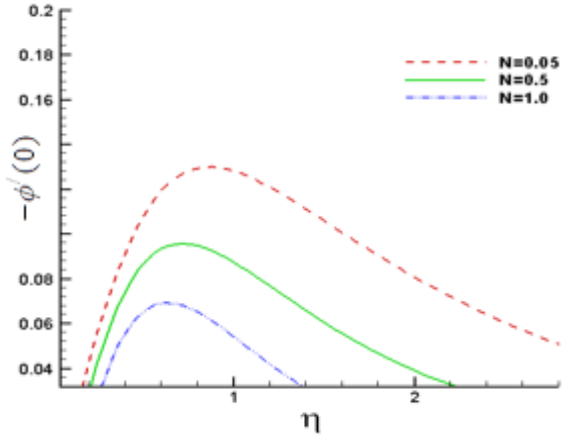

Figure 7. Impacts of various *N* on the rate of mass exchange.

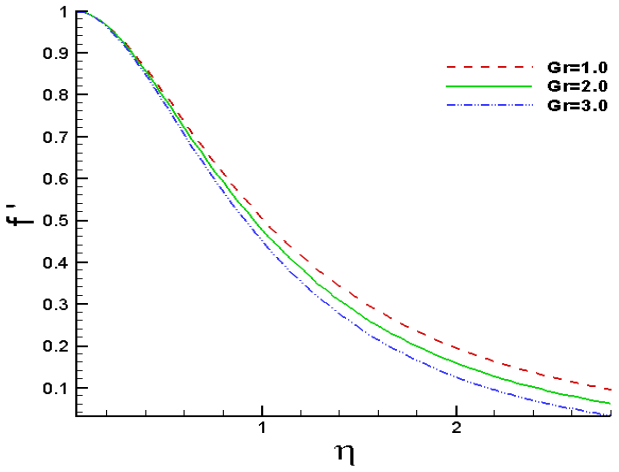

Figure 8. Impacts of various *Gr* on the field of velocity.

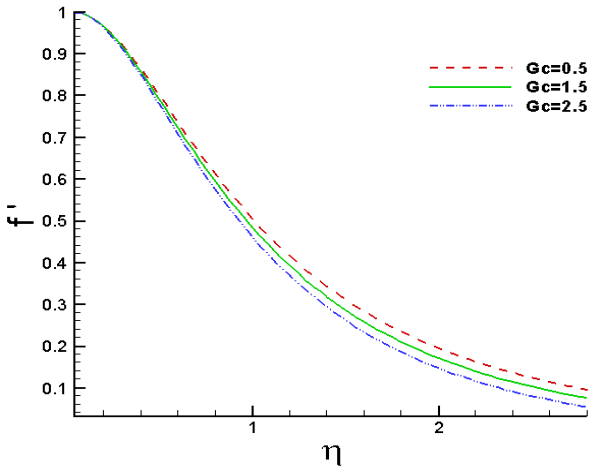

Figure 9. Impacts of various *Gc* on the field of velocity.

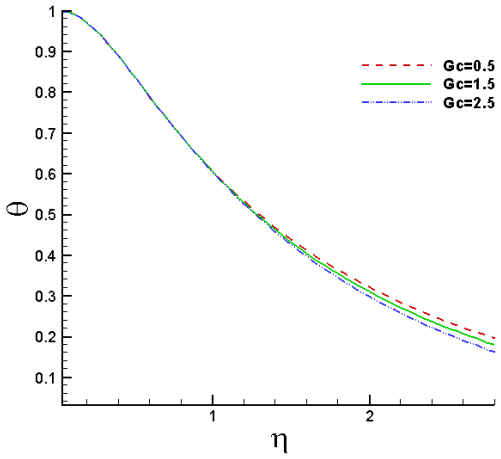

Figure 10. Impacts of various *Gc* on the field of temperature.

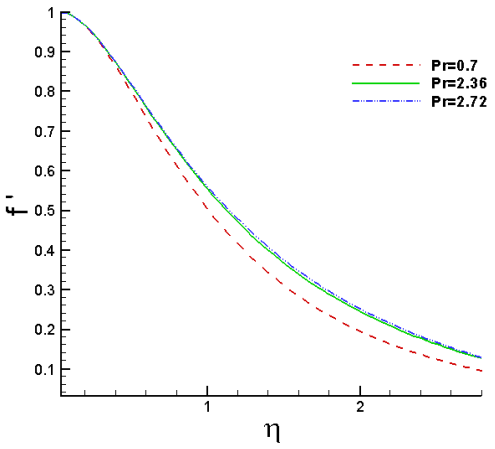

Figure 11. Impacts of various *Pr* on the field of velocity.

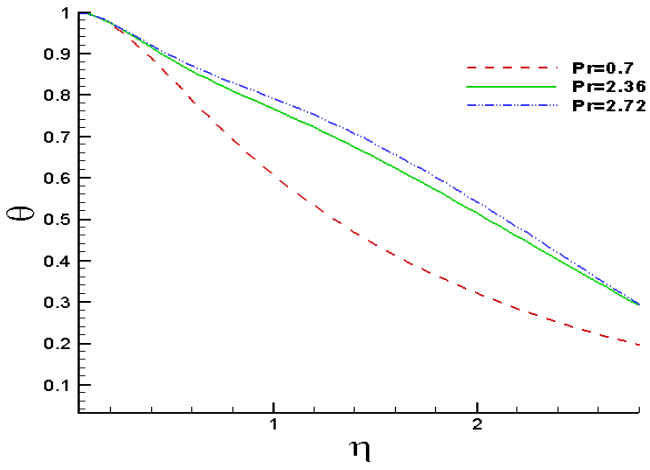

Figure 12. Impacts of various *Pr* on the field of temperature.

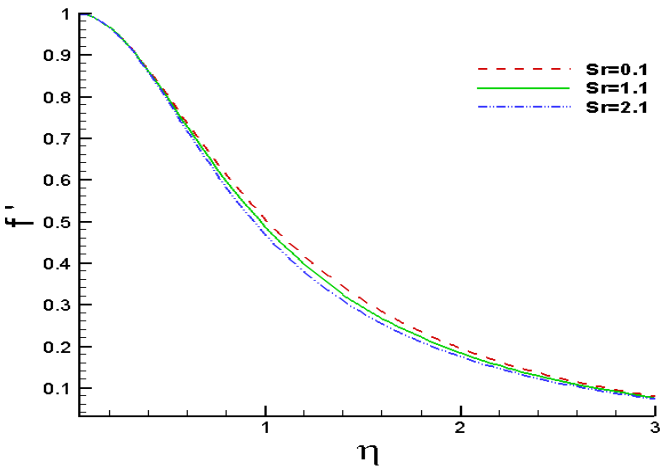

Figure 13. Impacts of various *Sr* on the field of velocity.

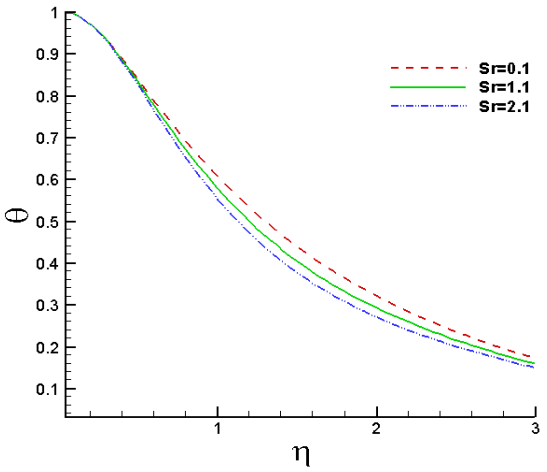

Figure 14. Impacts of various *Sr* on the field of temperature.

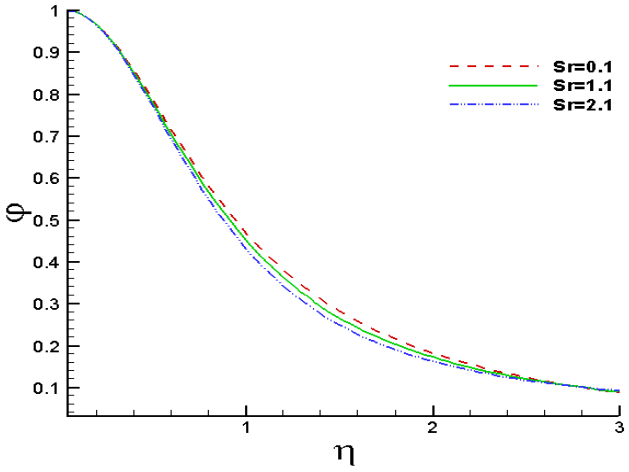

Figure 15. Impacts of various *Sr* on the field of concentration.

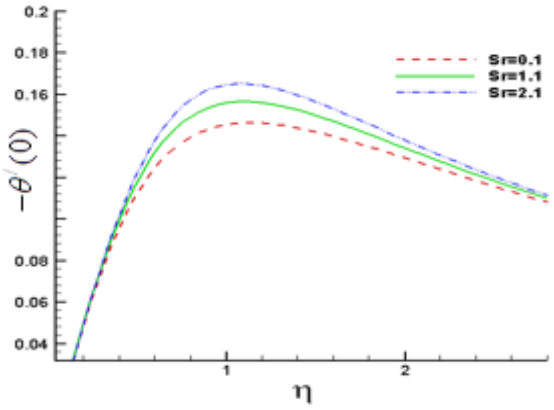

Figure 16. Impacts of various *Sr* on the rate of heat exchange.

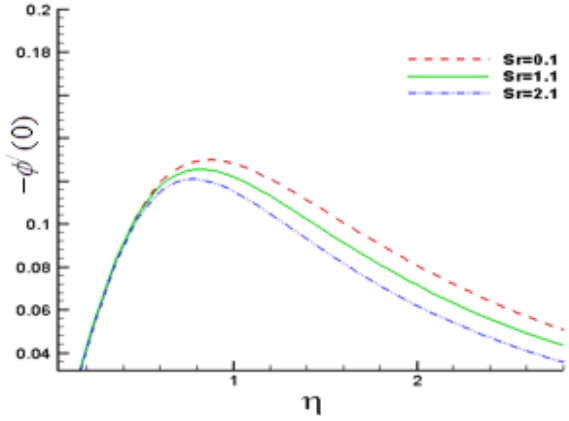

Figure 17. Impacts of various *Sr* on the rate of mass exchange.

Figures 16 and 17 put on view the impacts of Soret number on heat transfer rate and mass exchange rate respectively. Sherwood number falls and Nusselt number grows with the rise of Soret number. The heat exchange rate are 0.3955, 0.41696 and 0.4376 for *Sr = 0.1*, *Sr = 1.1* and *Sr = 2.1* for η = 0.6. The rate of decrement for *Sr = 0.1* to *Sr = 1.1* is 2.146% and rate of decrement for *Sr = 0.1* to *Sr = 2.1* is 2.064%. Sherwood numbers or rate of mass transfer are 0.37868, 0.372 and 0.3651 for *Sr = 0.1*, *Sr = 1.1* and *Sr = 2.1* for η = 0.6. For η = 0.6, the rate of decrement for *Sr = 0.1* to *Sr = 1.1* is 0.668% and rate of decrement for *Sr = 0.1* to *Sr = 2.1* is 0.69%.

5. Conclusions

This study presented the velocity, heat and mass exchange characteristics of Casson fluid via an inclined stretching plane. The governing system of nonlinear partial differential equations are changed into system of couple ordinary differential equations using similarity transformation. Numerical solutions to equations are used sixth order Runge-Kutta method along with Nachtsheim-Swigert shooting iteration technique. The impacts of a variety of non-dimensional variables on the field of flow, temperature and mass exchange are explained and then graphically depicted. The skin friction, rate of heat exchange and rate of mass exchange for different non-dimensional parameters are examined. The principal conclusions of this investigations are–

- Fluids flow, heat exchange, mass transfer and skin friction drops while Nusselt number and rate of mass exchange rises as Casson fluid parameter grows.
- As Soret number increases, field of the velocity, temperature, concentration as well as friction factor and Sherwood number fall but Nusselt number rises.
- The Grashof number (thermal) shows the decreasing behavior for velocity, Nusselt number

and increasing behavior for temperature, concentration, skin friction, Sherwood number.

- Velocity increases for the parameter of chemical reaction, exponential parameter, radiation parameter and Prandtl number drops for mass Grashof number, magnetic parameter.
- Temperature increases for chemical reaction parameter, mass Grashof number, magnetic parameter, exponential parameter, Prandtl number while falls for radiation parameter and Schmidt number.
- Concentration, Sherwood number decreases and skin friction, Nusselt number increases for concentration Grashof number.
- Skin friction increases for Prandtl number, chemical reaction parameter, magnetic parameter, exponential parameter and radiation parameter.
- For chemical reaction parameter and Prandtl number, the concentration, Nusselt number and rate of mass exchange decreases but for magnetic parameter and radiation parameter, mass exchange, Nusselt number and Sherwood number rises.
- Concentration and Sherwood number decreases and Nusselt number increases with the increase of exponential parameter and Schmidt number.
- For increasing the inclination of surfaces velocity, temperature and concentration increases then decreases.

Acknowledgement

The first author would like to gratefully acknowledge the financial support from Khulna University Authority to conduct this research work.

References

Alam, M.S., Rahman, M. M. and Samad, M.A. (2006). Numerical study of the combined free-forced convection and mass transfer flow past a vertical porous plate in a porous medium with heat generation and thermal diffusion. *Nonlinear Analysis: Modelling and Control*, 11 (4): 331-343.

Al-Obeide, I.H., Hammodat, A.A.R. (2020). New study of the stability of fluid flow in a porous channel under effects of magnetic field and radiation. *Open Access Library Journal*, 7.

Asogwa, K.K, Ibe, A.A. (2020). A study of MHD Casson fluid flow over a permeable stretching sheet with heat and mass transfer. *Journal of Engineering Research and Reports*, 16(2): 10-25.

Bali, R., Awasthi, U. (2012). A Casson fluid model for multiple stenosed artery in the presence of magnetic field. *Applied Mathematics*, 3: 436-441.

Haq, R.U., Nadeem, S., Khan, Z.H., Okedayo, T.G. (2014). Convective heat transfer and MHD effects on Casson nanofluid over a shrinking sheet. Central European Journal of Physics, 12(12): 862-871.

Hussanan, A., Salleh, M.Z., Tahar, R.M., Khan, I. (2014). Unsteady boundary layer flow and heat transfer of a Casson fluid past an oscillating vertical plate with Newtonian heating. *PloS ONE*, 9(10).

Kameswaran, P.K., Shaw, S., Sibanda, P. (2014). Dual solutions of casson fluid flow over a stretching or shrinking sheet. *Indian Academy of Sciences*, 39(6): 1573-1583.

Khalid, A., Khan, I., Shafie, S. (2015). Exact solutions for unsteady free convective flow of Casson fluid over an oscillating vertical plate with constant wall temperature. *Abstract and Applied Analysis*, 2015, Article ID 946350, 8 pages.

Khalid, A., Khan, I., Khan, A., Shafie, A. (2015). Unsteady MHD free convection flow of Casson fluid past over an oscillating vertical plate embedded in a porous medium. *Engineering Science and Technology, an International Journal*. http://dx.doi.org/10.1016/j.jestch. 2014. 12. 006.

Malik, M.Y., Naseer, M., Nadeem, S., Rehman, A. (2014). The boundary layer flow of Casson nanofluid over a vertical exponentially stretching cylinder. *Applied Nanoscience*, 4:869-873.

Nadeem, S., Haq, R.U., Akber, N.S., Khan, Z.H. (2013). MHD three-dimensional Casson fluid flow past a porous linearly stretching sheet. *Alexandria Engineering Journal*, 52: 577-582.

Nadeem, S., Mehmood, R., Akber, N.S. (2014). Optimized analytical solution for oblique flow of a Casson-nano fluid with convective boundary conditions. *International Journal of Thermal Sciences*, 78: 90-100.

Nadeem, S., Haq, R.U., Lee, C. (2012). MHD flow of a Casson fluid over an exponentially shrinking sheet. *Scientia Iranica*, 19(6): 1550-1553.

Parandhama, A., Raju, K.V.S., Raju, M.C. (2019). MHD Casson fluid flow through a vertical plate. *Journal of Computational and Applied Research*, 9(2): 343-350.

Pramanik, S. (2014). Casson fluid flow and heat transfer past an exponentially porous stretching surface in presence of thermal radiation. *Ain Shams Engineering Journal*, 5(1): 205-212

Raju, C.S.K., Sandeep, N., Sugunamma, V., Babu, M.J., Reddy, J.V.R. (2016). Heat and mass transfer in magnetohydrodynamics Casson fluid over an exponentially permeable stretching surface. *Engineering Science and Technology, an International Journal*, 19: 45-52.

Reddy, M.G. (2015). Unsteady radiative- convective boundary-layer flow pf a Casson fluid with variable thermal conductivity. *Journal of Engineering Physics and Thermophysics*, 88(1):236-246.

Reza-E-Rabbi, Sk., Ahmmed, S.F., Arifuzzaman, S.M., Sarker, T., Khan, M.S. (2020). Computational modelling of multiphase fluid flow behaviour over a stretching sheet in the presence of nanoparticles. *Engineering Science and Technology, an International Journal*, 23(3):605-617.

Sarojamma, G., Vasundhara, B., Vendabai, K. (2014). MHD Casson fluid flow, heat and mass transfer in a vertical channel with stretching walls. *International Journal of Scientific and Innovative Mathematical Reasearch*, 2(10): 800-810.

Saqib, M., Ali, F., Khan, I., Sheikh, N.A. (2016). Heat and mass transfer phenomena in the flow of Casson fluid over an infinite oscillating plate in the presence of first-order chemical reaction and slip effect. *Neural Computing and Applications*, 30(7) https://link. springer.com/article/10.1007/ s00521-016-2810-x.

Sarker, T., Rabbi, S.R., Arifuzzaman, S.M., Ahmed, R., Khan, M.S., Ahmmed, S.F. (2019). MHD radiative flow of Casson and Williamson nanofluids over an inclined cylindrical surface with chemical reactions effects. *International Journal of Heat and Technology*, 37(4):1117-1126.

Singh, A.K., Dikshit, C.K. (1988). Hydrodynamic flow past a continuously moving semi-infinite plate for large suction. *Astrophysics and Space Science*, 148: 249-256.

Sulochana, C., Aparna, S.R., Sandeep, N. (2021). Heat and mass transfer of magneto hydrodynamics Casson fluid flow over a wedge with thermal radiation and chemical reaction. *Heat transfer*, 50: 3704-3721.

Vijaya, N., Sreelakshmi, K., Sarojamma, G. (2016). Effect of magnetic field on the flow and heat transfer in a Casson thin film on an unsteady stretching surface in the presence of viscous and internal heating. *Open Journal of Fluid Dynamics*, 6: 303-320.

Wahiduzzaman, M., Islam, M.T., Sultana, P., Afikuzzaman, M. (2014). MHD couette flow of a Casson fluid between parallel porous plates. *Progress in Nonlinear Dynamics and Chaos*, 2(2):51-60.